Surfaces, Interfaces, and Changing Shapes in Multilayered Films

Daniel Josell and Frans Spaepen

Introduction

It is generally recognized that the capillary forces associated with internal and external interfaces affect both the shapes of liquid-vapor surfaces and wetting of a solid by a liquid. It is less commonly understood that the same phenomenology often applies equally well to solid-solid or solid-vapor interfaces.

The fundamental quantity governing capillary phenomena is the excess free energy associated with a unit area of interface. The microscopic origin of this excess free energy is often intuitively simple to understand: the atoms at a free surface have "missing bonds"; a grain boundary contains "holes" and hence does not have the optimal electronic density; an incoherent interface contains dislocations that cost strain energy; and the ordering of a liquid near a solid-liquid interface causes a lowering of the entropy and hence an increase in the free energy. In what follows we shall show how this fundamental quantity determines the shape of increasingly complex bodies: spheres, wires, thin films, and multilayers composed of liquids or solids. Crystal anisotropy is not considered here; all interfaces and surfaces are assumed isotropic.

Drops

Spherical Drop

Consideration of the equilibrium of a spherical drop of radius R with surface free energy γ shows that pressure inside the droplet is higher than outside. The difference is given by the well-known Laplace equation:

$$\Delta P = \frac{2\gamma}{r}. \qquad (1)$$

This result can be obtained by equating work done against internal and external pressure during an infinitesimal change of radius with the work of creating a new surface. By considering the mechanical equilibrium (i.e., no net force) of a portion of the same droplet obtained by a planar cut, the surface free energy is seen to be equivalent to a force-per-unit-length pulling in a plane tangent to the surface and perpendicular to the edge (see Figure 1a). In this way it cancels the force associated with the pressure difference between inside and outside. The surface free energy is therefore also referred to as the surface tension.

By considering volume-conserving perturbations of the surface, one can show that in equilibrium the sum K_T of the two principal curvatures must be uniform over the entire surface. For a sphere, the principal curvatures are $1/r$, and their sum $2/r$ is constant over the entire surface. Comparison to Equation 1 shows that $\Delta P = K_T\gamma$, a result that is generally valid.*

*This discussion applies only to fluids. For an isotropic solid sphere, Equation 1 becomes $\Delta P = 2f/r$, where f is the surface stress. The surface tension is the work to create a unit area at constant strain; the surface stress is related to the work to strain the surface elastically. For fluids,[1,2] $f = \gamma$. For the equilibrium shape problems in this article, the relevant quantity is still the interface tension, even for solids if there is sufficient plastic deformation (usually diffusional) to permit creation and elimination of interfaces at constant strain. If the solid particles are larger than about 10 nm, the bulk values of the interfacial tensions can be used. For smaller particles, the strains induced by the interface stress may shift the value of the interfacial tension slightly.

Consider a junction (Figure 1b) of three interfaces with interface free energies that are independent of orientation. The equilibrium configuration, found by requiring that a virtual displacement of the triple junction causes no change in the total interface free energy, corresponds to that for which the net force on the junction from the tensions of the interfaces is zero.

Liquid Drop on a Solid Surface

In the absence of gravity, a liquid drop on a solid surface has the shape of a spherical cap (constant curvature) and contacts the surface at an angle determined by the free energies of the three interfaces. At a fixed volume of liquid, the radius of the spherical cap and the height of the center of the corresponding sphere relative to the surface are uniquely determined. If the solid surface is rigid and planar (Figure 1c), the contact angle is determined by balancing just the forces parallel to the surface. (Note: This

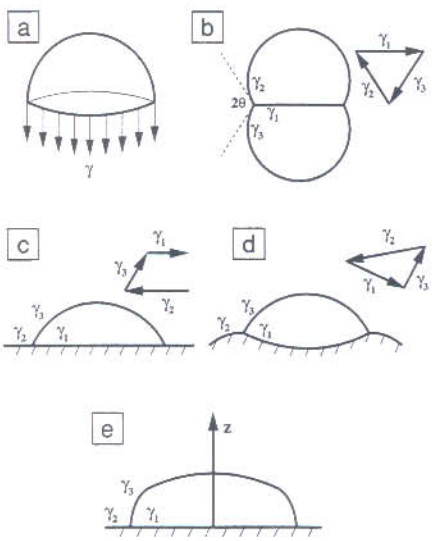

Figure 1. (a) Surface tension acting on the perimeter of a half drop. (b) Junction of three surfaces or interfaces characterized by a groove angle θ; the vector representations of the surface tensions add up to zero. (c) Wetting of a rigid surface by a liquid drop; only the tangential components of the tensions add up to zero. (d) Wetting of a plastically deformable surface; the junction of the interfaces adjusts itself to make the full vector sum of the tensions zero. (e) In a gravitational field, the local curvature of the surface becomes a function of the height, z. γ_i is the interfacial tension for interface i.

is true locally for nonplanar surfaces too.) The perpendicular component of the forces is balanced by elastic stresses in the solid. If the surface is deformable, both components of the forces must balance, as in Figure 1d. Measurements of the angles are often used to determine relative values of interfacial tensions.

If gravity cannot be neglected, the curvature of the surface is no longer constant. Instead, $K_T\gamma + \rho gz$ must be constant over the surface, where ρ is the density, g is the acceleration due to gravity, and z is the height (see Figure 1e.). This condition is obtained from requiring the chemical potential to be independent of position. The surface free energy can be obtained from this "sessile drop" experiment by measuring the dependence of the surface curvature on the height if the density of the fluid is known.

Wire

Consider now wire, modeled in Figure 1b as a stack of linked drops (now solid), which can be subjected to an axial load. The "bamboo" structure shown in Figure 2a is found in well-annealed wires. Each truncated sphere represents a single grain; the groove where two droplets join represents a grain boundary. If the drops are truly truncated spheres, with the grain length fixed by the grain volume and radius, no net axial force exists because surface and pressure terms cancel.

In the general case, where the length of the grain is independent of the grain volume and radius, the total curvature K_T is still constant over the surface, but the two principal curvatures are unequal and vary with position. In this case, the pressure and surface tension forces do not cancel. This means that a nonzero net axial force F is necessary for equilibrium. The value of the equilibrium force is unique for the geometry. This force, together with grain dimensions and grain-boundary groove angles (see Figure 2a) obtained by microscopy, gives a direct measure of the free energy of the wire surfaces.[3]

Such experiments were first used 50 years ago to obtain the surface free energies of Ag, Cu, and Au wires in their vapor.[4,5] In practice, the strain rate is measured for different applied forces; positive strain rates are observed for larger forces and negative ones for small (but still tensile) forces (see Figure 2b). Since the plastic deformation mechanism in these experiments is diffusional creep, the force corresponding to zero strain rate can be accurately determined by a linear interpolation. The free energy of the grain boundaries γ_{gb} can be obtained from the surface free energy γ_{fs} and the grain-boundary groove angle 2θ according to the triple-junction equilibrium: $\gamma_{gb} = 2\gamma_{fs}\cos(\theta)$.

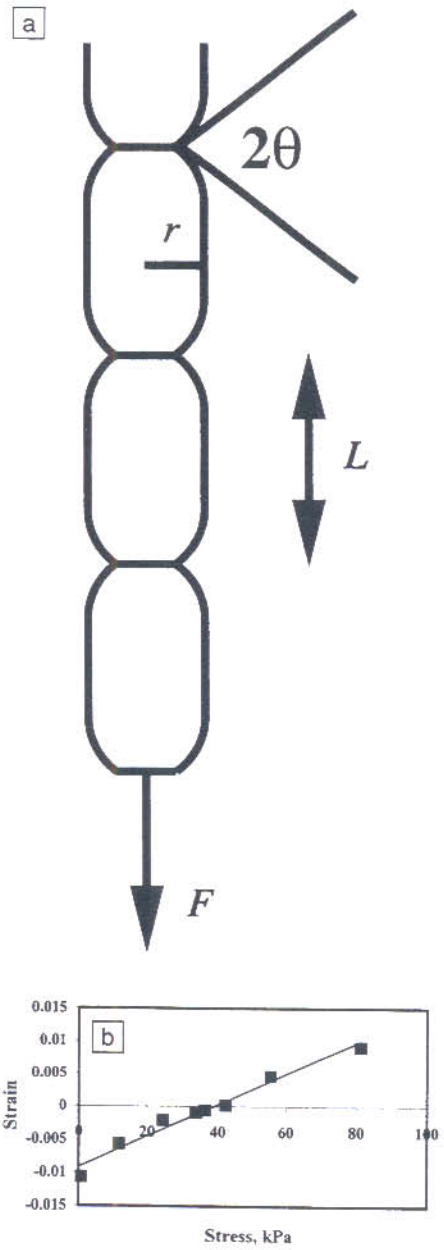

Figure 2. (a) A wire with a bamboo grain structure; F is a nonzero net axial force, L is length of one grain, r is the radius, and 2θ is the grain-boundary groove angle. (b) Cumulative strains, both positive and negative, of Cu wires (after 72 h at 1000°C) after axial creep at different stresses.[4]

Thin Films and Multilayers

The equilibrium geometry of thin films and multilayers can be found by a similar approach. If the layers are single crystals or amorphous, the surfaces and interfaces are flat and generate a biaxial force (per width of film, see Figure 3a) parallel to the plane of the film. In a biaxial creep experiment, the force per width at which the specimen exhibits zero strain rate (zero creep) corresponds to the sum of the free energies of the parallel surfaces and interfaces.† As in the case of the wire, spherical caps form the equilibrium surface of a thin film with grains that can be modeled as a regular two-dimensional array, (e.g., of hexagons). Figure 3b shows the example of a bubble raft (i.e., linked, truncated spheres). The triple junctions form pits that under certain conditions can perforate the film. When the in-plane equilibrium force is zero, interface free energy minimization at constant volume again determines the radius of curvature and the height of the center of the corresponding sphere (Figure 3b). However, unlike for the wire, the general equilibrium surface with a nonzero equilibrium load is still a spherical cap. The nonzero equilibrium force arises in the foil by an increase or decrease in the height of the center of the spherical cap (Figure 3b), which leads to, respectively, an increase or decrease of the contribution of the *pressure* term through the area over which it acts. The interfaces within multilayered films are also sections of truncated spherical caps when the grains in each layer are modeled by a regular square or hexagonal array (Figure 3c).

The capillary forces associated with the interfaces between layers in a multilayer establish a biaxial zero-creep force. (For a typical multilayer, the number of interfaces is sufficiently large that the contributions of any free surface[s] and the multilayer/substrate interface are negligible.) This force can be estimated as follows. An interface free energy of 1 J/m^2 produces 1 N force for each interface in a meter-wide specimen. For layers with thickness $d = 1\ \mu$m, the corresponding equilibrium biaxial stress γ/d is 1 MPa. For $d = 1$ nm, the stress rises to 1 GPa. The capillary forces associated with the grain boundaries within the layers decrease this value.

†In case of elastic deformation (as opposed to plastic deformation in creep experiments) the force per width is equal to the sum of the surface and interface stresses. This force is opposed by elastic stresses, either by bending of the substrate[6] or deformation of the film, if freestanding.[7]

the following estimates of the time constants for shape relaxation along each of the paths. For lattice diffusion:

$$\tau_L = \frac{r^3 kT}{D_L \gamma \Omega} \quad (2)$$

where D_L is the lattice diffusion coefficient. For surface diffusion:

$$\tau_S = \frac{r^4 kT}{D_S \delta \gamma \Omega} \quad (3)$$

where $D_S\delta$ is the (experimentally directly accessible) product of the surface diffusivity and the effective thickness of the diffusion layer. For vapor transport:

$$\tau_V = \frac{r^2 (2\pi m)^{1/2} (kT)^{3/2}}{p \gamma \Omega^2} \quad (4)$$

where m is the atomic mass.

Surface diffusion, with a time constant proportional to r^4, is dominant for small grains (smallest time constant means fastest process). Vapor transport, with a time constant proportional to r^2, is dominant for large grains. Since, generally for a given system, the activation energy for the vapor pressure is greater than that for the lattice diffusivity, which in turn is greater than that for the surface diffusivity, one expects these processes to dominate in that order with decreasing temperature. Table I[12] gives examples for 20-pm-diameter particles of Cu and W at their respective melting temperatures. In Cu of this size, vapor transport never dominates, whereas in W it is the dominant mechanism at the melting temperature.

Figure 5b illustrates the diffusion paths leading to shape relaxation in multilayers by grain-boundary grooving. In the initial stage of relaxation, when the groove depth h is still small compared to the distance d' between the grain boundaries, its evolution is described by treatment[13] of grain-boundary grooving at a free surface. The only difference is that vapor transport does not occur and that grain-boundary diffusion takes the place of surface diffusion. At these short distances lattice diffusion can be ignored. A simple dimensional analysis gives an estimate of the evolution with time, t:

$$h^4 = \frac{D_B \delta \gamma \Omega}{kT} t \quad (5)$$

where $D_B\delta$ is the (experimentally accessible) product of the grain-boundary diffusivity and thickness. Note the similarity to Equation 3.

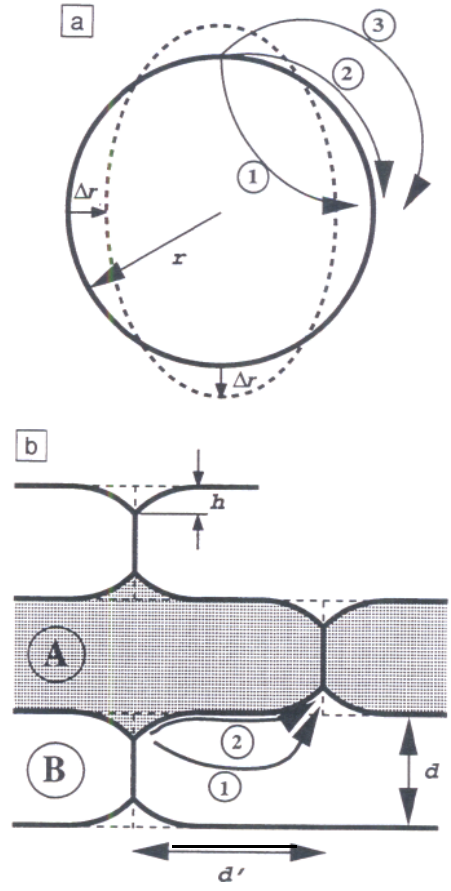

Figure 5. (a) Kinetic paths for shape relaxation of an isotropic particle; r is *the radius of the spherical equilibrium shape;* Ar *is the maximum displacement away from the equilibrium shape. (1) lattice diffusion; (2) surface diffusion; and (3) vapor transport. (b) Kinetic paths for late-stage shape relaxation in multilayers (1) lattice diffusion; and (2) grain-boundary (interface) diffusion, where* h *is the* groove *depth,* d *is the layer thickness, and* d' *is the distance between grain boundaries.*

Table I: Deformation-Mechanism-Dependent Relaxation Times*

Path	Cu	W
Lattice	1.2 x 10^9	4.3 x 10^9
Surface	1.2 x 10^9	2 x 10^9
Vapor	2 x 10'	1.5 x 10^9

'Shape relaxation times (in s) for 20-μm-diameter Cu and W particles at their respective melting temperatures according to Equations 2-4. Data from a compilation by Swinkels and Ashby.[12]

When the depth of the grain-boundary groove is of similar magnitude as the layer thickness *d*, the chemical potential gradient driving diffusion becomes established between adjacent boundaries over a distance d' instead of a distance h in the early stages. Note that in many microstructures $d' \approx d$. At the same time, bulk diffusion has to be considered as a possible contributor. Equation 5 therefore becomes modified as:

$$h^3 = (D_L d + D_G \delta) \frac{\gamma \Omega}{dkT} t. \quad (6)$$

The temperature determines which type of diffusion dominates. For example, for $d = 1$ μm in Cu, $D_L d = D_G \delta$ at 1300 K; for $d = 10$ μm the temperature is 1046 K. This is consistent with Coble creep as the dominant deformation mechanism in the zero-creep experiments discussed earlier in this section.' By setting $h = d$ in Equation 6, one can obtain an estimate of the time it takes to complete the grooving process. For 1-μm Cu at 1000 K, the relaxation time is about 10^9 s. This again is consistent with the time scale of the zero-creep experiments.

Stability

Equilibrium interface shapes and applied forces were discussed in the first three sections. However some grain shapes and/or dimensions permit interface shapes that, though they have constant curvature and satisfy groove angle requirements, are not stable to perturbations. There are also geometries for which constant curvature shapes simply do not exist. These two conditions, along with inappropriate applied forces, lead to three types of instabilities that can degrade a thin film or a multilayer: (1) the action of equilibrium forces that decrease with increasing sample size; (2) the action of applied forces that are inconsistent with the capillary forces; and (3) the absence of a continuous minimal surface consistent with the volumes and in-plane dimensions of the grains."

The first instability manifests itself as coarsening: the growth of large grains at the expense of smaller ones (grain growth). The second is the basis of the zero-creep experiments used to measure surface and interfacial free energies; application of forces other than the equilibrium values leads to nonzero strain rates.

The third instability, which applies to local grain dimensions and groove angles, is most immediately destructive. It was noted in the section on thin films and multilayers that the shapes of equilibrated interfaces in continuous films and multi-

the following estimates of the time constants for shape relaxation along each of the paths. For lattice diffusion:

$$\tau_L = \frac{r^3 kT}{D_L \gamma \Omega} \quad (2)$$

where D_L is the lattice diffusion coefficient. For surface diffusion:

$$\tau_S = \frac{r^4 kT}{D_S \delta R} \quad (3)$$

where $D_S\delta$ is the (experimentally directly accessible) product of the surface diffusivity and the effective thickness of the diffusion layer. For vapor transport:

$$\tau_V = \frac{r^2 (2\pi m)^{1/2} (kT)^{3/2}}{p\gamma\Omega^2} \quad (4)$$

where m is the atomic mass.

Surface diffusion, with a time constant proportional to r^4, is dominant for small grains (smallest time constant means fastest process). Vapor transport, with a time constant proportional to r^2, is dominant for large grains. Since, generally for a given system, the activation energy for the vapor pressure is greater than that for the lattice diffusivity, which in turn is greater than that for the surface diffusivity, one expects these processes to dominate in that order with decreasing temperature. Table I[12] gives examples for 20-pm-diameter particles of Cu and W at their respective melting temperatures. In Cu of this size, vapor transport never dominates, whereas in W it is the dominant mechanism at the melting temperature.

Figure 5b illustrates the diffusion paths leading to shape relaxation in multilayers by grain-boundary grooving. In the initial stage of relaxation, when the groove depth h is still small compared to the distance d' between the grain boundaries, its evolution is described by treatment[13] of grain-boundary grooving at a free surface. The only difference is that vapor transport does not occur and that grain-boundary diffusion takes the place of surface diffusion. At these short distances lattice diffusion can be ignored. A simple dimensional analysis gives an estimate of the evolution with time, t:

$$h^4 = \frac{D_B \delta \gamma \Omega}{kT} t \quad (5)$$

where $D_B\delta$ is the (experimentally accessible) product of the grain-boundary diffusivity and thickness. Note the similarity to Equation 3.

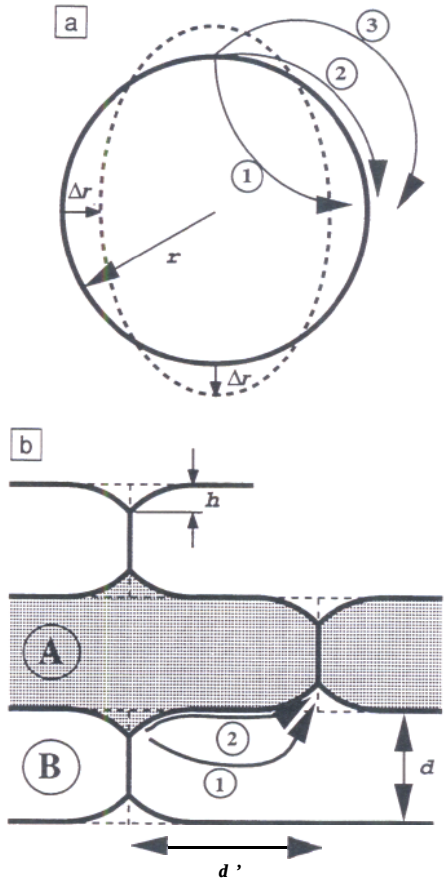

Figure 5. (a) Kinetic paths for shape relaxation of an isotropic particle; r is *the radius of the spherical equilibrium shape;* Ar *is the maximum displacement away from the equilibrium shape. (1) lattice diffusion; (2) surface diffusion; and (3) vapor transport. (b) Kinetic paths for late-stage shape relaxation in multilayers: (1) lattice diffusion; and (2) grain-boundary (interface) diffusion, where* h *is the groove depth,* d *is the layer thickness, and* d' *is the distance between grain boundaries.*

Table I: Deformation-Mechanism-Dependent Relaxation Times*

Path	Cu	W
Lattice	1.2×10^6	4.3×10^9
Surface	1.2×10^9	2×10^9
Vapor	2×10^7	1.5×10^5

'Shape relaxation times (in s) for 20-μm-diameter Cu and W particles at their respective melting temperatures according to Equations 2-4. Data from a compilation by Swinkels and Ashby.[12]

When the depth of the grain-boundary groove is of similar magnitude as the layer thickness d, the chemical potential gradient driving diffusion becomes established between adjacent boundaries over a distance d' instead of a distance h in the early stages. Note that in many microstructures $d \approx d$. At the same time, bulk diffusion has to be considered as a possible contributor. Equation 5 therefore becomes modified as:

$$h^3 = (D_L d + D_G \delta) \frac{\gamma\Omega}{dkT} t \quad (6)$$

The temperature determines which type of diffusion dominates. For example, for $d = 1$ μm in Cu, $D_L d = D_G \delta$ at 1300 K; for $d = 10$ μm the temperature is 1046 K. This is consistent with Coble creep as the dominant deformation mechanism in the zero-creep experiments discussed earlier in this section.[8] By setting $h = d$ in Equation 6, one can obtain an estimate of the time it takes to complete the grooving process. For 1-μm Cu at 1000 K, the relaxation time is about 10^5 s. This again is consistent with the time scale of the zero-creep experiments.

Stability

Equilibrium interface shapes and applied forces were discussed in the first three sections. However some grain shapes and/or dimensions permit interface shapes that, though they have constant curvature and satisfy groove angle requirements, are not stable to perturbations. There are also geometries for which constant curvature shapes simply do not exist. These two conditions, along with inappropriate applied forces, lead to three types of instabilities that can degrade a thin film or a multilayer: (1) the action of equilibrium forces that decrease with increasing sample size; (2) the action of applied forces that are inconsistent with the capillary forces; and (3) the absence of a continuous minimal surface consistent with the volumes and in-plane dimensions of the grains."

The first instability manifests itself as coarsening: the growth of large grains at the expense of smaller ones (grain growth). The second is the basis of the zero-creep experiments used to measure surface and interfacial free energies; application of forces other than the equilibrium values leads to nonzero strain rates.

The third instability, which applies to local grain dimensions and groove angles, is most immediately destructive. It was noted in the section on thin films and multilayers that the shapes of equilibrated interfaces in continuous films and multi-

layers composed of regular arrays of grains can be generated from sections of spherical caps. However a continuous solution consistent with the grain volumes, dimensions, and groove angles of a particular material does not always exist. In its mildest form, this causes limited "pinchoff" at the triple junctions between grains. In more severe cases, it may lead to complete separation at grain boundaries and the development of a granular film. The range of behaviors of different creep samples was seen in Figure 4: some maintained a layered structure for long testing times; others suffered pinchoff before exhibiting any significant creep deformation. For the reasons discussed in the section on kinetics, these stability issues become especially relevant as the layers become thinner, and are the likely origin of the granular nature of Ag/$Ni_{80}Fe_{20}$ multilayers studied for their giant magnetoresistance.[14]

Even though pinchoff in polycrystalline layers is directly related to the presence of the grain boundaries (since it occurs at the triple junctions where they meet within the layers), the problem would be much worse in the absence of grain-boundary grooves. If these grooves are (inappropriately) neglected, infinitely deep perforations are predicted.[15] In reality, the triple junctions in regular arrays of grains equilibrate at finite depth and do not perforate the film[10,16] (unlike Mullins' isolated grain-boundary groove[13]). The development of these grooves causes stagnation of coarsening (grain growth) in thin films and multilayers by "anchoring" the boundary at the bottom of the groove." This stagnation process ultimately stabilizes films and multilayers against perforation since pits would eventually form when the in-plane grain size becomes much larger than the film or layer thickness.[11,16]

Acknowledgment

D. Josell's work is supported in part by Contract No. DE-FG02–97ER45664 from the OBES at DOE. F. Spaepen's work in this area is supported by the National Science Foundation through the Harvard MRSEC under Contract No. DMR-94–*00396.*

References

1. R.C. Cammarata, *Prog.* Surf. Sci. 46 (1994) p. 1.
2. J.W. Cahn, *Acta Met. 28 (1980)* p. 1333.
3. D. Josell, *Acta Metall. Mater. 41 (1993)* p. 2179.
4. H. Udin, A.J. Shaler, and J. Wulff, Trans. *AIME J. Met. 1 (1949)* p. 186.
5. H. Udin, *ibid. 3* (1951) p. 63.
6. J.A. Ruud, A. Witvrouw, and F. Spaepen, *J. Appl. Phys. 74* (1993) p. 2517.
7. J. Weissmüller and J.W. Cahn, *Acta Mater.* 45 (1997) p. 1899.
8. D. Josell and F. Spaepen, *Acta Metall. Mater. 41* (1993) p. 301%
9. D. Josell and Z.L. Wang, in *Thin Films: Stresses and Mechanical Properties* V, edited by S.P. Baker, C.A. Ross, P.H. Townsend, C.A. Volkert, and I'. Bsrgesen (Mater. Res. Soc. Symp. Proc. 356, Pittsburgh, 1995) p. 357.
10. D. Josell and WC. Carter, in *Creep and Stress Relaxation in Miniature Components,* edited by H.D. Merchant (The Minerals, Metals, & Materials Society, Warrendale, PA, 1997) p. 271.
11. D. Josell, W.C. Carter, and J.E. Bonevich, *Proceedings of 4th Int. Conf. on Nanostructured Materials* to be published in the *Journal of Nanostructured Materials.* In press.
12. F.B. Swinkels and M.F. Ashby, *Acta* Met. 29 (1981) p. 259.
13. W.W. Mullins, *J. Appl. Phys. 28* (1957) p. 333.
14. R.D. McMichael, P.J. Chen, and W.F. Egelhoff, Jr., IEEE *Trans. Magn. 34 (1998)* p. 89%
15. D.J. Srolovitz and S.A Safran, *J. Appl. Phys. 60* (1986) p. 247.
16. D. Josell, S.R. Coriell, and G. McFadden, *Acta Metall. Mater. 43* (1995) p. 1987.
17. W.W. Mullins, *Acta Met. 6* (1958) p. 414. □

Cost Effective Portable Spin Coaters

Two-Stage Spinning
Dispense liquid during Stage 1;
spin-up and flatter during Stage 2.

Adjustable Speed
Stage 1: 500 - 2,500 rpm
2 - 18 second
Stage 2: 1,000 - 8,000 rpm
3 - 60 second

Precision Benchtop Dip Coaters

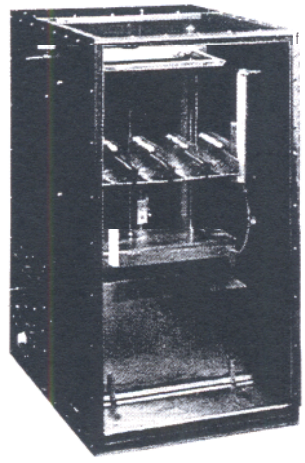

Robust Laboratory Coater
Easy to operate
Speed Range 0 - 30 cm/min
Adjustable Travel Span
Controllable Atmosphere
Infrared Drying
Custom Fabrication

Coatings
Available for
Metal Oxides,
Nitrides & Carbides

VISIT MRS BOOTH NO. 214 216

CHEMAT TECHNOLOGY, INC.
9036 Winnetka Ave., Northridge, CA 91324
(818) 727-9786, Fax: (818) 727-9477, e-mail: chemat@aol.com
Distributorships Available Worldwide

Circle No. 6 on Reader Service Card.